Am J Cancer Res 2024;14(6):2805-2822
www.ajcr.us /ISSN:2156-6976/ajcr0155918

Original Article

Extracellular putrescine can augment the epithelial-mesenchymal transition of gastric cancer cells by promoting MAL2 expression by elevating H3K27ac in its promoter region

Chenxiao Bi[1], Chengyu Li[1], Liangxiu Xing[2], Zixuan Lu[2], Haiyan Liu[1], Tao Hu[2], Bin Wang[2], Chengxia Liu[1]

[1]*Department of Gastroenterology and Institute of Digestive Disease, Binzhou Medical University Hospital, Binzhou 256600, Shandong, China;* [2]*Department of Immunology, Binzhou Medical University, Yantai 264000, Shandong, China*

Received February 15, 2024; Accepted May 20, 2024; Epub June 15, 2024; Published June 30, 2024

Abstract: Dysregulation of polyamine metabolism has been associated with the development of many cancers. However, little information has been reported about the associations between elevated extracellular putrescine and epithelial-mesenchymal transition (EMT) of gastric cancer (GC) cells. In this study, the influence of extracellular putrescine on the malignant behavior and EMT of the AGS and MKN-28 cells was investigated, followed by RNA sequencing profiling of transcriptomic alterations and CUT&Tag sequencing capturing H3K27ac variations across the global genome using extracellular putrescine. Our results demonstrated that the administration of extracellular putrescine significantly promoted the proliferation, migration, invasion, and expression of N-cadherin in GC cells. We also observed elevated H3K27ac in MKN-28 cells but not in AGS cells when extracellular putrescine was used. A combination of transcriptomic alterations and genome-wide variations of H3K27ac highlighted the upregulated *MAL2* and H3K27ac in its promoter region. Knockdown and overexpression of *MAL2* were found to inhibit and promote EMT, respectively, in AGS and MKN-28 cells. We demonstrated that extracellular putrescine could upregulate *MAL2* expression by elevating H3K27ac in its promoter region, thus triggering augmented EMT in GC cells.

Keywords: Putrescine, gastric cancer, H3K27ac, *MAL2*, CUT&Tag

Introduction

Gastric cancer (GC) was responsible for over one million new cases and 769,000 deaths, ranking fifth in global incidence and mortality in 2020 [1]. Epithelial-mesenchymal transition (EMT) and tumor metabolic microenvironment were recognized to contribute significantly to influencing GC [2, 3]. During EMT, epithelial cells undergo a phenotypic switch by the loss of expression of their epithelial markers (E-cadherin) and become mesenchymal cells by the acquisition of expression of mesenchymal markers (N-cadherin) [4]. Current research has demonstrated close associations between polyamine dysregulation and cancer progression [5]. Additionally, many studies have indicated conflicting roles of polyamine in EMT. For instance, Marco *et al*. [6] have revealed a direct link between the depletion and activation of endoplasmic reticulum stress and the enhancement of EMT in MDCK cells. In addition, overexpression of the polyamine-affected *MYC* gene increased the expression of Snail and Vimentin and decreased E-cadherin levels in the HSC3 cells [7, 8]. Cellular polyamines are derived from endogenous organisms, dietary, and intestinal microbes [9]. Dietary polyamines, one of the significant sources of exogenous polyamines, can readily be absorbed in the intestinal lumen and subsequently function within the body [10].

Moreover, post-translational modifications (including acetylation, methylation, ADP ribosylation, and phosphorylation) of histone proteins, specifically H3-H4, have been linked to EMT in several cancers. Dynamic changes in H3K27ac and H3K27me3 induce the splicing modifica-

https://doi.org/10.62347/BEUV4081

tions seen during EMT [11]. In GC, despite the promoting roles of Wnt/β-catenin and P13K/Akt signaling pathways in EMT via H3K27ac [12], little is known about how H3K27ac affects the occurrence of EMT in GC. Furthermore, the increased expressions of ornithine decarboxylase (ODC) and polyamines are hallmarks of epithelial tumorigenesis [13]. Studies have shown that polyamines might influence histone acetyltransferase (HAT) and histone deacetylase (HDAC) activity [14, 15], suggesting that polyamines may regulate EMT through H3K27ac.

Most investigations have focused on spermine and spermidine rather than putrescine, likely because spermine and spermidine are derivatives of putrescine. However, emerging studies have demonstrated the direct roles of putrescine in regulating cellular activities. For instance, supplementing putrescine instead of spermidine and spermine could reduce the percentage of infected macrophages in macrophage metabolism [16]. The level of putrescine can directly affect the broiler chicks' hatchability, gut morphology, and pre-production performance [17]. Considering the established relationship between the gut microbiome and GC [18] and that putrescine is one of the metabolites of gut microorganisms [19], it was found that putrescine, as opposed to spermine and spermidine, promoted DNA synthesis [20]. In particular, *Helicobacter pylori*, a known carcinogenic intestinal microorganism for GC, is a significant putrescine producer [21, 22]. This has prompted our interest in investigating the connections between extracellular putrescine, H3K27ac levels throughout the entire genome, the EMT phenotypes in gastric cancer cells, and the underlying mechanisms.

In this study, we aimed to explore 1) whether putrescine could promote EMT in MKN-28 and AGS cell lines, 2) the alteration in H3K27ac levels across the global genome, and 3) the alterations in transcriptomes in the two cell lines. We aimed to uncover the underlying mechanisms, which would be verified through gene overexpression and knock-out experiments in the cell lines. We found that putrescine might promote EMT through the H3K27ac-MAL2 axis. Our findings will deepen the relationship between polyamine metabolism and cancer and contribute to understanding the involvement of the polyamine-rich diet in gastric cancer progression.

Materials and methods

Tumor cell lines and culture conditions

We selected MKN-28 cell lines with high E-cadherin and low N-cadherin expressions and AGS cell lines with high N-cadherin and low E-cadherin expressions to explore the effect of putrescine on EMT of GC cells *in vitro* [23]. The human AGS and MKN-28 cell lines were purchased from the Procell Life Science & Technology Co., Ltd., Nanjing, China. The GC cells were cultured in RPMI 1640 medium supplemented with 10% fetal bovine serum (FBS, Procell Life Science & Technology Co., Ltd.) and 1% penicillin/streptomycin (Procell Life Science & Technology Co., Ltd.). All cell lines were maintained at 37°C, 5% CO_2.

HPLC assay of putrescine

Three parallel groups were set up for each concentration of putrescine. The AGS and MKN-28 cells were cultured with 1640 medium containing 0, 500, and 1000 ng/mL of putrescine. The cell supernatants were collected before and after 24 h and stored at -20°C. The standard putrescine was purchased from Sigma-Aldrich (99%). The sample was derivatized with NaOH (2 mol/L), saturated $NaHCO_3$, NH_3H_2O, acetonitrile acetonitrile (chromatographically pure), and dansulfonyl chloride (10 mg/mL). After derivatization, the samples were filtered with an oil-water 0.22 μm filter (Biosharp, Guangzhou, China) for High-Performance Liquid Chromatography (HPLC) analysis. A chiral HPLC was performed on a Wooking K2025 HPLC (High performance liquid chromatography) system (Shandong Wooking Instruments, Shandong, China) with a Sunniet C18 end-capped column (250 mm × 4.6 mm, 5 μm). The mobile phase comprised acetonitrile (chromatographically pure) (A) and 5 mmol/L aqueous formic ammonium acetate (B). The gradient elution was as follows: 0-5 min, 60% A; 5-12 min, 60-75% A; 12-20 min, 75-95% A; 20-20.1 min, 95-60% A; 20.1-30 min, 60% A. The flow rate was kept at 1.0 mL/min. The temperature of the column was maintained at 30°C, and the injection volume of the solute was 10 μL. The chromatograms were recorded every 30 min.

Estimation of malignant behavior of GC cells using cell proliferation, cell migration, invasion, and cell wound-healing assays

According to the manufacturer's instructions, the cell counting kit-8 (CCK-8) assays were used to determine cell proliferation (Elabscience Biotechnology Co., Ltd.). In the 96-well plates with 2×10^4 cells/well, the AGS/MKN-28 cells were cultured for 12 h (37°C, 5% CO_2) and then treated with gradient concentrations (0, 125, 250, 500, and 1000 ng/mL) of putrescine for additional 24 h. For the CCK-8 assay, 10 μL/well of CCK-8 solution was added and incubated at 37°C for 1.5 h. The absorbance (optical density, OD) of cells was measured at 450 nm using a microplate reader (TECN). The cell growth curves were plotted using time on the horizontal axis and absorbance on the vertical axis.

The cell migration/invasion assay was determined using a 24-well Boyden chamber with an 8-mm pore-size polycarbonate membrane (Corning, Union City, CA, USA). An appropriate volume of Matrigel (1:8) was added to the upper chamber of the Transwell plates for the invasion assay. The plates without Matrigel in the upper chamber were used for the migration assay. The cell suspension (1×10^5 cells/100 μL serum-free MEM media) was added to the upper chambers, and a 700 μL complete culture medium containing 10% FBS was added to the lower chambers. The cells were incubated for 48 h (37°C, 5% CO_2). The cells were washed with PBS three times, fixed in 4% paraformaldehyde for 30 min, and stained with 0.1% crystal violet for 20 min. Next, five regions were randomly chosen under the microscope to take representative photographs and count the cells.

The cell wound healing assay was performed as described previously [24]. The cells were cultured at 37°C, 5% CO_2. Photographs of the scratch wound in different samples were recorded at 0 and 48 h. The expressions of E-cadherin and N-cadherin of AGS and MKN-28 cells were quantified using Western blot.

Western blot

Total protein was extracted from the cells using a RIPA buffer with a protease inhibitor (MedChemExpress, Monmouth, NJ, USA) and a phosphatase inhibitor cocktail (Beyotime, Shanghai, China). The protein concentration was measured by using a BCA kit (Beyotime). The proteins were separated through electrophoresis using 12% and 10% SDS-PAGE and transferred onto a polyvinylidene fluoride (PVDF) membrane (Millipore, Billerica, MA, USA). Then, the samples were blocked with 10% nonfat milk (Solarbio, Beijing, China) for 2 h and immunoblotted with the primary antibodies overnight at 4°C. After being washed three times with TBST buffer, the protein bands were incubated with the corresponding secondary antibodies for 2 h at room temperature and then probed with appropriate horseradish peroxidase (HRP-conjugated secondary antibody, Elabscience Biotechnology Co., Ltd.) and visualized using chemiluminescence (Elabscience Biotechnology Co., Ltd.). Antibodies used in this study were: Anti-GAPDH (1:1000 dilution, Abmart), anti-Tubulin (1:1000 dilution, Abmart), anti-H3 (1:8000 dilution, ProteinTech), anti-H3K27ac (1:50000 dilution, Abcam), anti-H3K27me3 (1:50000 dilution, Abcam), anti-E-cadherin (1:50000 dilution, ProteinTech), anti-N-cadherin (1:8000 dilution, ProteinTech), and anti-MAL2 (1:1000 dilution, Bioss). The intensity of the protein bands was determined using ImageJ software.

Library construction, sequencing, and data analysis of transcriptome and CUT&Tag

The group sets for constructing transcriptome and CUT&Tag libraries were Put0 (0 ng/mL), Put500 (500 ng/mL), and Put1000 (1000 ng/mL) for both AGS and MKN-28 cells based on the concentrations of putrescine. The library construction, sequencing, and data analysis of the transcriptome and CUT&Tag were performed as in our previous study [25]. After extracting the total RNA for transcriptomes using an ALLPure DNA/RNA/Protein Kit (CW-BIO, Cat.CW0591S) according to the manufacturer's instructions. The transcriptome libraries were constructed using a VAHTS® Universal V8 RNA-seq Library Prep Kit for Illumina (Vazyme Biotech Co., Ltd.). The quantified libraries using qPCR were sequenced on a NovaSeq 6000 platform in Novogene (Beijing, China). The raw reads were filtered using the fastp software [26]. The clean reads were then aligned against the GRCh38 genome dataset, and a gene-sample count table was constructed by employing

the Subread software [27]. Differential gene analysis and variance stabilizing transformation (VST) were performed using DESeq2 [28] for downstream analysis, which included gene set enrichment analysis (GSEA) against the Molecular Signatures Database (MSigDB 7.5.1) using the clusterProfiler package (version 4.4.2) [29, 30]. The time series gene expression was clustered using the Mfuzz package [31].

The CUT&Tag library was constructed using the Hyperactive® Universal CUT&Tag Assay Kit (Vazyme Biotech Co., Ltd., China). A total of 1 × 10^5 cells per sample were processed with the anti-H3K27ac antibody and the input control IgG. The library was then quantified using qPCR and sequenced on a NovaSeq 6000 platform at Novogene (Beijing, China). Fastp and Bowtie2 [32] were employed to filter the raw reads and align the clean reads against the GRCh38 genome dataset, respectively. Following that, spike-in normalization, summarizing the fragment size distribution, calling peak using MACS2 software, and annotating peaks with the ChIPseeker package [33] were performed. The differential analysis, GSEA, and Mfuzz clustering of the promoters were performed similar to transcriptomic analysis.

Examining the roles of MAL2 in EMT of AGS and MKN-28

The Flag-MAL2 and shRNAs (shMAL2-1#, shMAL2-2#, and shMAL2-3#) were synthesized using Applied Biological Materials (Vancouver, Canada). They were then employed to produce different lentiviral particles in 293T cells. After 24 h transfection, the cell culture medium was replaced with a fresh DMEM medium. The cell culture medium containing the viral particles was collected after 72 h and used to transduce GC cells. Then, selected cells were treated with puromycin (1.5 μg/mL for MKN-28 and 1 μg/mL for AGS) for 72 h, and the infection efficiency was observed using inverted fluorescence microscopy. The expressions of *MAL2*, E-cadherin, and N-cadherin of AGS and MKN-28 cells were quantified using Western blot.

CUT&RUN-qPCR

As described above, the AGS and MKN-28 cells were divided into control (NC) and Putrescine groups (1000 ng/mL). Following the manufacturer's instructions, A hyperactive pG-MNase CUT&RUN Assay Kit for PCR/qPCR (Vazyme Biotech Co., Ltd., China) was employed to assess the abundance of H3K27ac in the promoter region of *MAL2* using 10^5 input cells, anti-H3K27ac antibody (ABclonal, Shanghai, China), and the primers for qPCR (F-5'-TGAGCCAAGACCACACTATTGC-3' and R-5'-GCCATCTTTGCTTTGCCTCTCC-3'). The antibody anti-IgG (ABclonal) was used for the negative control. The kit contained a total of 15 ng of spike-in DNA, along with its corresponding primer pairs. The relative enrichment fold was determined by the $2^{-\Delta\Delta Ct}$ method as follows:

$$\triangle CT_{Putrescine} = CT_{Putrescine} - CT_{Spike\text{-}in\ DNA\ in\ Putrescine}$$

$$\triangle CT_{NC} = CT_{NC} - CT_{Spike\text{-}in\ DNA\ in\ NC}$$

$$\triangle CT_{IgG} = CT_{IgG} - CT_{Spike\text{-}in\ DNA\ in\ IgG}$$

Then,

$$REF_{Putrescine} = 2^{-(\triangle CT_{Putrescine} - \triangle CT_{IgG})}$$

$$REF_{NC} = 2^{-(\triangle CT_{NC} - \triangle CT_{IgG})}$$

Where *REF* is the abbreviation of relative enrichment fold.

Tumor-bearing mouse model establishment

The male BABL/c nude mice (5-week-old) (Ji'nan Pengyue Laboratory Animal Breeding Co., LTD., China) were divided into NC, Putrescine, and Putrescine+C646 groups (n = 5). All animal experiments were performed as approved by the ethics committee of Binzhou Medical University (20240130-45). A total of 1 × 10^7 cells of AGS or MKN-28 in 100 μL were inoculated into the back of BABL/c nude mice. The tumor growth was monitored by using a ruler every day. Around three days later, when the tumor size was almost 60 mm^3, 20 ng putrescine in 100 μL PBS and 10 μM C646 (Absin, Shanghai, China) were injected into the xenograft tumors daily. After seven days, the mice were euthanized to collect tumors for subsequent analyses. The total protein for Western Blot was extracted as described above.

Statistical analysis

Statistical analysis was performed using GraphPad Prism 9.5. All the data were expressed as mean ± standard deviation (SD).

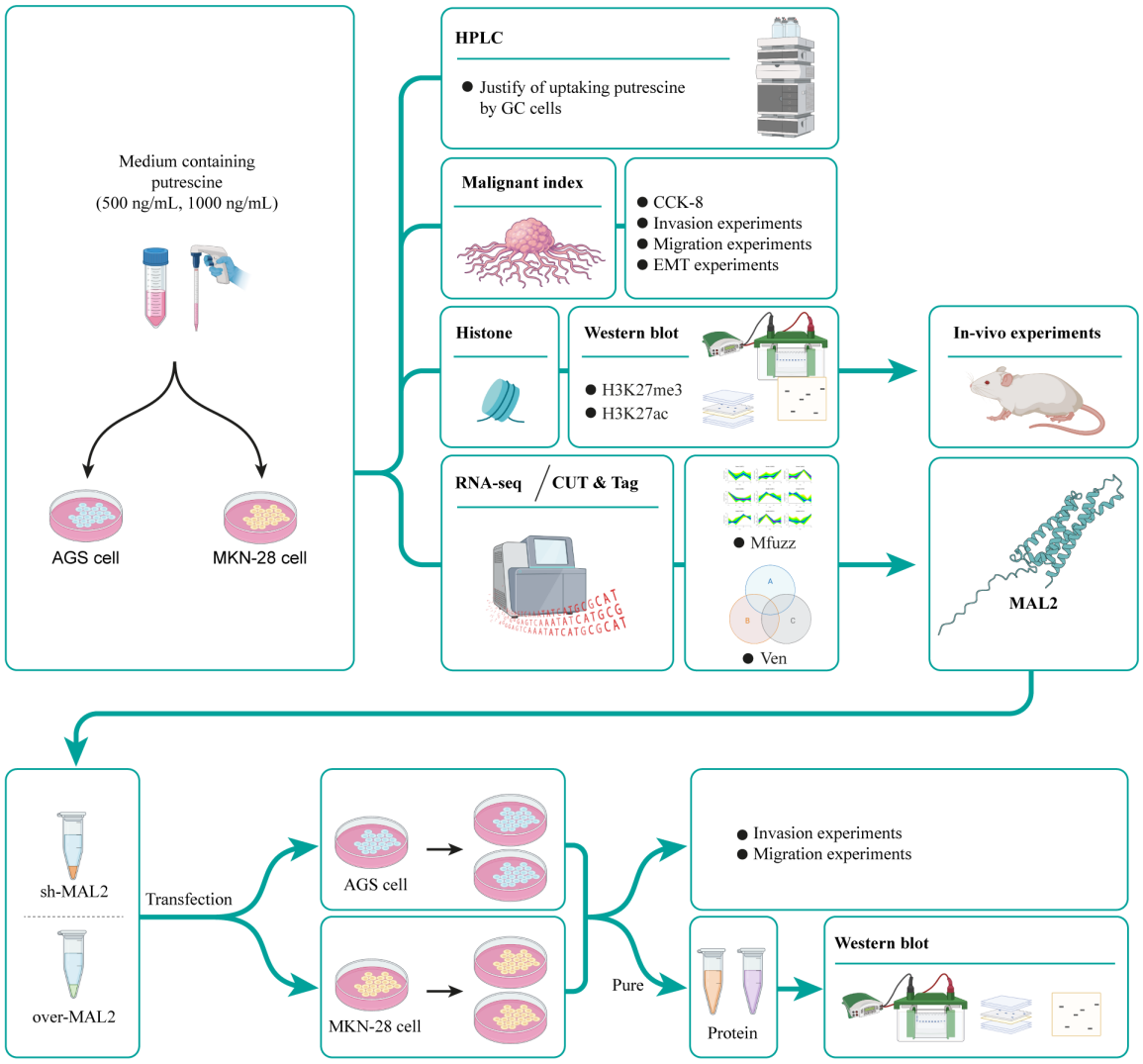

Figure 1. The schematic diagram of experimental plan.

Comparisons between two groups were assessed by *t*-test, and a two-way ANOVA was used to analyze the significance of multiple comparisons between the groups. $P < 0.05$ was considered statistically significant.

Results

Extracellular putrescine augmented the malignant behavior of GC cells

The schematic diagram of the experimental plan in this study is shown in **Figure 1**. HPLC was employed to quantify the putrescine concentration in the supernatant after incubation to estimate the uptake of extracellular putrescine by GC cells. The peak retention time of standard putrescine was 15.467 min (**Figure 2A**). The standard curve based on the gradient concentration of standard putrescine (0, 10, 25, 50, 75, and 100 ng/mL) was generated to determine the putrescine concentrations in samples (**Figure 2B**). AGS and MKN-28 were treated with 500 and 1000 ng/mL of putrescine. The putrescine concentration in the supernatant of MKN-28 continuously decreased for three days, while the supernatant putrescine in AGS was reduced to and then stabilized at around 50% after one day of incubation (**Figure 2C**), demonstrating the consumption of extracellular putrescine by the proliferating AGS and MKN-28 cells.

The effects of extracellular putrescine on the malignant behavior of AGS and MKN-28 cells

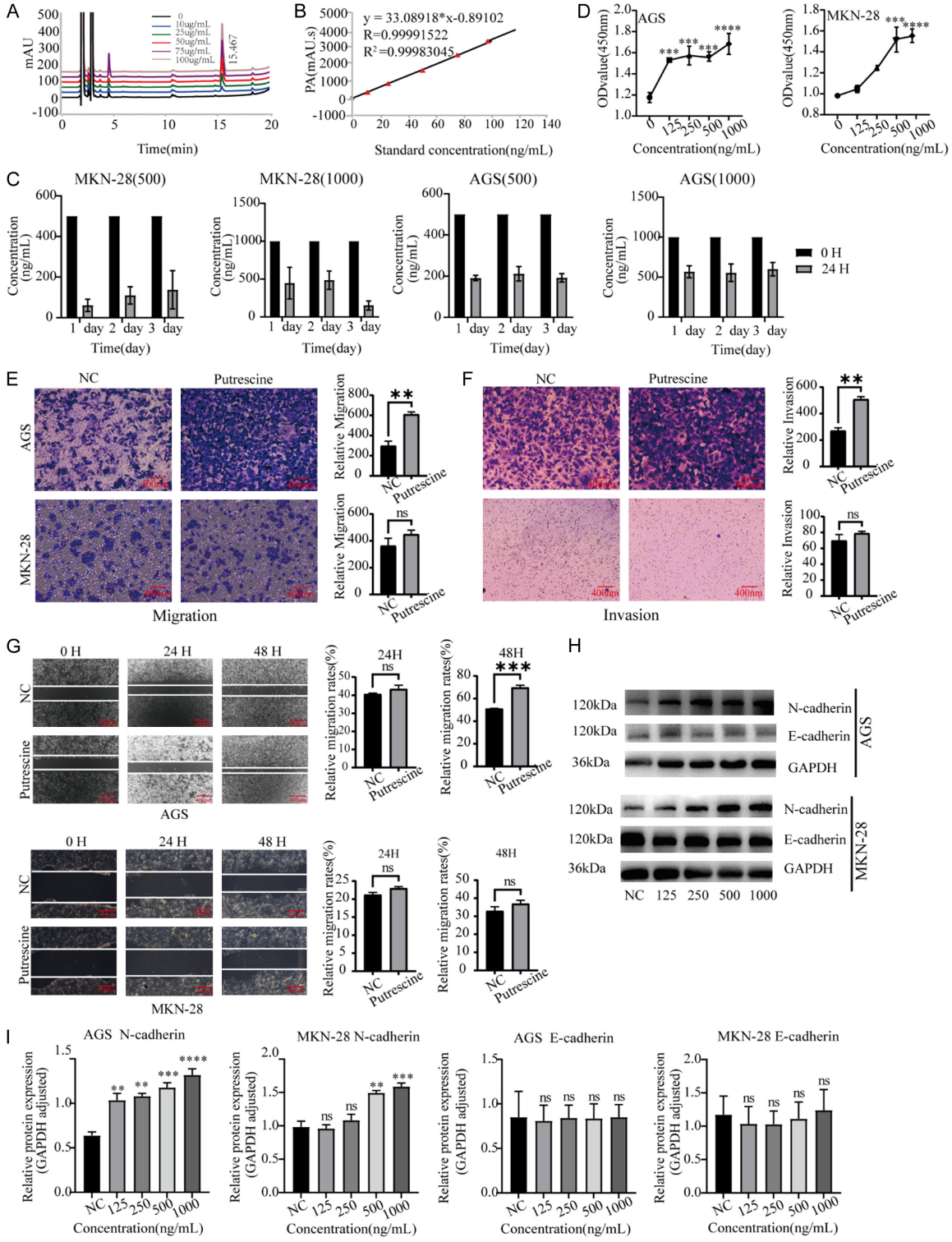

Figure 2. The effect of putrescine on malignant behavior of gastric cancer cells. A. Chromatogram of the eluted peaks for putrescine standards; B. Linearity curves for putrescine; C. HPLC showing extracellular putrescine uptake in gastric cancer AGS and MKN-28 cells; D. CCK-8 assay showed the viability of AGS and MKN-28 cells with increasing concentrations of exogenous putrescine; E, F. The migration and invasion of AGS and MKN-28 cells was investigated by transwell assay; G. Wound healing assay showed the ability of migration in AGS and MKN-28 cells; H, I. E-cadherin and N-cadherin protein levels were testified with western blot. Experiments were conducted in triplicate. Data are shown as mean ± SD. **P* < 0.05, ***P* < 0.01, and ****P* < 0.001.

were subsequently investigated. The CCK-8 analysis showed that the cell proliferation, as measured by the OD values at 450 nm, of the AGS and MKN-28 cells increased significantly with the addition of extracellular putrescine. This indicates that putrescine promotes the proliferation of GC cells (**Figure 2D**). Transwell Matrigel invasion and scratch assays were conducted to study the effects of putrescine on the invasion and migration of GC cells. **Figure 2E-G** demonstrates that AGS cells, but not MKN-28 cells, exhibited notably higher migration and invasion in response to 1 μg/mL extracellular putrescine (Putrescine group) compared to NC. Western blot was employed to study the effect of putrescine on the expression of N-cadherin and E-cadherin in AGS and MKN-28 cells. Significantly upregulated N-cadherin with increased concentration of extracellular putrescine was observed in both AGS and MKN-28 cells ($P < 0.05$, **Figure 2H** and **2I**).

Transcriptomic variations in AGS and MKN-28 in extracellular putrescine administration

Next, we investigated the effects of extracellular putrescine on AGS and MKN-28 cells at the transcriptomic level. Using variance stabilizing transformation to normalize the data, principal component analysis (PCA) revealed 47.91% and 44.53% variance in the first three axes of AGS and MKN-28 cells, respectively. This suggests that the Put500 and Put1000 in AGS cells were separate clusters (**Figure 3A**; **Table 1**). The types of currently known 1184 EMT-related genes, including "Dual roles genes", "Oncogenic genes", and "Suppressive genes", were referred from *dbEMT2* [34]. Following that, pairwise differential comparisons were conducted to elucidate the EMT genes that were either upregulated or downregulated (**Figure 3B**), demonstrating a gradual increase in differentially expressed genes (DEGs) with the rise in extracellular putrescine concentration compared to the NC group in AGS. However, the number of DEGs in MKN-28 was much lower than in AGS. We simultaneously observed upregulated and downregulated oncogenic and suppressive genes in both cell lines. Moreover, GSEA indicated that the DEGs of Put1000 vs NC in AGS could be enriched into upregulated cellular respiration-related pathways (such as "Oxidative Phosphorylation") (**Figure 3C**). Based on the investigation, it was reasonable to hypothesize that some unknown genes in GC cells are promoted by putrescine, in addition to the already verified EMT gene, *dbEMT2*. Therefore, the Mfuzz package was employed to characterize the dynamic changes at the gene expression level with an increasing extracellular putrescine concentration. Nine tendency patterns were observed in both AGS and MKN-28 cells (**Figure 3D**). However, the Venn diagram illustrated that the number of genes shared between an AGS cell and an MKN-28 cell in each category was significantly smaller than the number of unique genes in each cell line.

Genome-wide alteration of H3K27ac caused by extracellular putrescine

Then, we investigated the effect of putrescine on the genome-wide alteration of H3K27ac and H3K27me3. There was no notable disparity in the levels of H3K27me3 between MKN-28 and AGS cells. However, the presence of putrescine significantly promoted the expression of H3K27ac in MKN-28 cells but not in AGS cells (**Figure 4A**). H3K27ac can be inhibited by histone acetylation inhibitor C646 [35]. To determine the roles of H3K27ac and putrescine in GC, the mice bearing AGS and MKN-28 cells were treated with putrescine and putrescine+C646. The tumor size of mice in the Putrescine group was significantly larger than the NC and Putrescine+C646 groups (**Figure 4B**). In both AGS-bearing and MKN-28-bearing mice, the expression of N-cadherin was elevated in the Putrescine group compared to the NC, but C646 impaired such increment in the Putrescine+C646 group (**Figure 4C**), suggesting that putrescine might promote EMT of GC by elevating H3K27ac.

CUT&Tag was then employed to study the alteration of H3K27ac levels across the global genome when different concentrations of extracellular putrescine were administered (0, 500, and 1000 ng/mL). The concentration maps of CUT&Tag illustrated that the peak-out enrichment regions of H3K27ac were concentrated in the TSS region, and the H3K27ac peaks increased with increasing putrescine concentrations (**Figure 4D**). Additional gene annotation revealed that most H3K27ac-

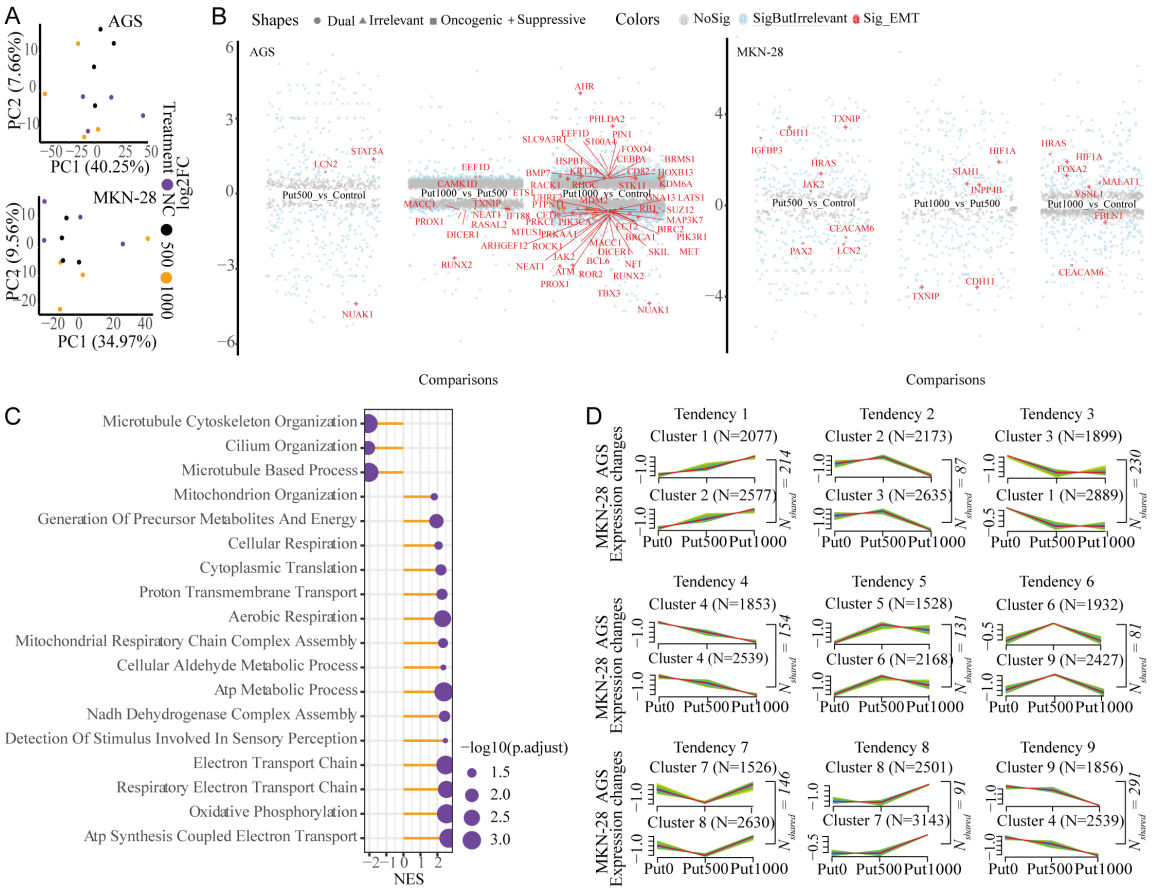

Figure 3. The RNA-seq analysis of exogenous putrescine (0, 500, and 1000 ng/mL) on AGS and MKN-28 cells. A. Principal component analysis was performed on all groups of AGS and MKN-28 cells. Each dot represents one biological replicate; B. A Volcano plot depicting the different gene expressions at three concentrations of putrescine in AGS and MKN-28 cells. EMT genes that have a significant relationship are highlighted in red, while EMT genes that are significant but not relevant are highlighted in blue; C. A Lolly plot illustrating the significantly enriched pathways using DEGs in Put1000 vs Control in AGS, and GSEA against GOBP database. No significant enrichment was observed in MKN-28 cells; D. The diagrams illustrate the patterns of dynamic-changed genes and the different concentrations of exogenous putrescine in AGS and MKN-28 cells, using Mfuzz. The N_{shared} means the number of genes shared between AGS and MKN-28 cells with the same tendency.

Table 1. The data from PCA analysis for transcriptome

	Group 1	Group 2	Mean	SD	*p* value
AGS	1000	500	49.91652	9.969248	0.032
	1000	NC	54.08015	15.925340	0.438
	500	NC	46.70879	6.768881	0.408
MKN-28	1000	500	44.10973	9.934635	0.552
	1000	NC	48.68518	10.350567	0.532
	500	NC	43.15742	5.387995	0.148

modified reads are highly concentrated in the promoter region. However, the percentage of promoter regions bonded with H3K27ac decreased gradually in AGS cells and increased gradually in MKN-28 cells as the concentrations of putrescine increased (**Figure 4E**).

PCA based on total and promoter features showed that putrescine concentration was responsible for most of the variance (**Figure 4F**; **Table 2**). In addition, the PCA analysis using promoter features showed a similar pattern to the PCA analysis using total features. However, it exhibited a slightly higher total variance in the first three axes. This suggests that the impact of putrescine on the overall changes in H3K27ac was mainly concentrated in the promoter regions of the genome.

To determine the dynamics of H3K27ac in promoter regions after extracellular putrescine administration, Mfuzz was employed and as-

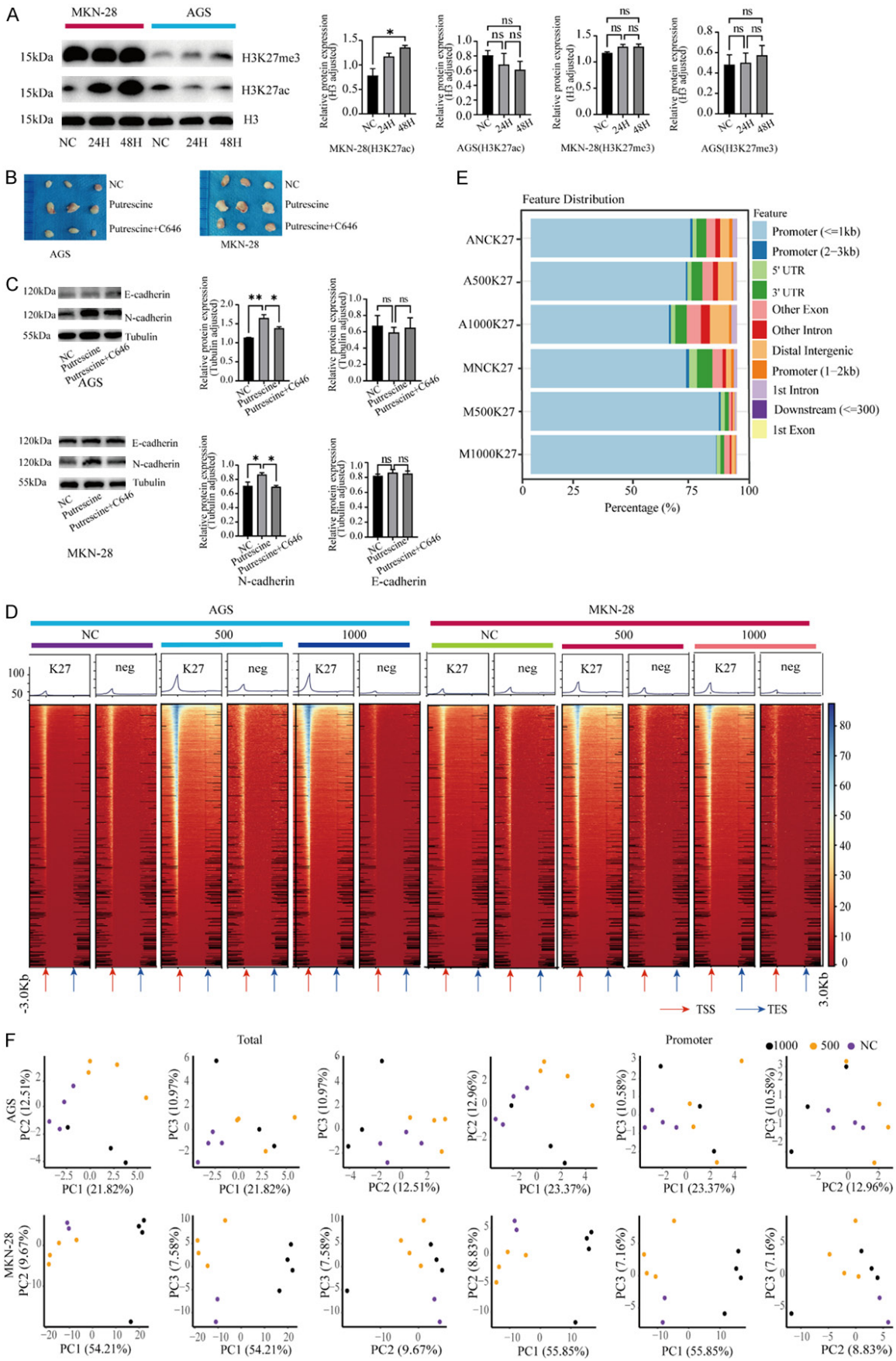
A
MKN-28
AGS
15kDa
H3K27me3
15kDa
H3K27ac
15kDa
H3
NC 24H 48H NC 24H 48H
Relative protein expression (H3 adjusted)
MKN-28(H3K27ac)
AGS(H3K27ac)
MKN-28(H3K27me3)
AGS(H3K27me3)
B
NC
Putrescine
Putrescine+C646
AGS
MKN-28
C
120kDa
E-cadherin
120kDa
N-cadherin
55kDa
Tubulin
Relative protein expression (Tubulin adjusted)
N-cadherin
E-cadherin
D
AGS
MKN-28
NC
500
1000
K27
neg
-3.0Kb
3.0Kb
TSS
TES
E
Feature Distribution
Feature
Promoter (<=1kb)
Promoter (2–3kb)
5' UTR
3' UTR
Other Exon
Other Intron
Distal Intergenic
Promoter (1–2kb)
1st Intron
Downstream (<=300)
1st Exon
ANCK27
A500K27
A1000K27
MNCK27
M500K27
M1000K27
Percentage (%)
F
Total
Promoter
1000
500
NC
AGS
MKN-28
PC1 (21.82%)
PC2 (12.51%)
PC3 (10.97%)
PC1 (23.37%)
PC2 (12.96%)
PC3 (10.58%)
PC1 (54.21%)
PC2 (9.67%)
PC3 (7.58%)
PC1 (55.85%)
PC2 (8.83%)
PC3 (7.16%)

Figure 4. CUT&Tag capturing genome-wide alteration of H3K27ac in AGS and MKN-28 cells under the administration of different concentrations of extracellular putrescine (0, 500, and 1000 ng/mL). A. H3K27ac and H3K27me3 protein levels were determined by Western blot. Experiments were conducted in triplicate; B. Tumors were removed and photographed five days after injection; C. The protein expression levels of E-cadherin and N-cadherin were detected by Western blot in tumors; D. Heatmaps showing the genomic occupancy of input and H3K27ac ± 3 kb flanking TSSs and TESs in AGS and MKN-28 cells treated with different concentrations of exogenous putrescine; E. The genome-wide distribution of H3K27ac binding regions under the influence of putrescine; F. PCA was performed on all groups of total H3K27ac and promoter H3K27ac in AGS and MKN-28 cells. Each dot represents one biological replicate. Experiments were conducted in triplicate. Data are shown as mean ± SD. $*P < 0.05$, $**P < 0.01$, and $***P < 0.001$.

Table 2. The data from PCA analysis for CUT&Tag

	Group 1	Group 2	Mean	SD	*p* value
AGS-Promoter	1000	500	7.557216	0.5119962	0.164
	1000	NC	7.280633	0.4753735	0.030
	500	NC	7.564662	0.8629471	0.032
MKN-28-Promoter	1000	500	30.10324	2.9207460	0.034
	1000	NC	28.00522	0.8652562	0.070
	500	NC	18.05172	1.3972331	0.402
AGS-Total	1000	500	10.15873	0.6282401	0.178
	1000	NC	10.01170	0.5819764	0.020
	500	NC	10.06187	1.0379790	0.052
MKN-28-Total	1000	500	40.95501	3.5213860	0.028
	1000	NC	37.95548	0.9048678	0.068
	500	NC	24.81161	1.8144831	0.258

signed all the promoters into nine tendency patterns (**Figure 5A**). As observed in transcriptomes, the Venn diagram comparing AGS and MKN-28 cells showed a smaller overlap of shared genes than cell-specific genes. This suggests significant differences between AGS and MKN-28 cells. In tendency 3, there was significantly decreased in Put1000 compared to Put500. Most of the genes involved in this tendency were enriched in pathways related to protein-folding, assisted explicitly by the eukaryotic chaperonin TRiC/CCT and the Rho family (**Figure 5B**).

Subsequently, we examined if any common essential genes were involved in the increased EMT caused by putrescine by enhancing H3K27ac in the promoter regions in both AGS and MKN-28 cells. Genes from clusters that tended toward increase were isolated and classified into the following groups: RNA-AGS (transcriptomic genes in Cluster 1 and 8 of AGS cells), Promoter-AGS (promoters in Cluster 4 and 8 of AGS cells), RNA-MKN-28 (transcriptomic genes in Cluster 2 and 7 of MKN-28 cells), and Promoter-MKN-28 (promoters in Cluster 7 and 9 of MKN-28 cells). The Venn diagram within the four groups identified three genes they shared: *GPI*, *TRPS1*, and *MAL2* (**Figure 5C**). Considering the opposing roles of *GPI* and *TRPS1* in several studies [36-39]. We prioritized *MAL2* in further exploration. H3K27ac peaks were validated at the *MAL2* promoter region, marking increasing H3K27ac peaks with increasing concentrations of putrescine (**Figure 5D**), which was verified by CUT&RUN-qPCR using a primer of the *MAL2* promoter region (**Figure 5E**). Therefore, we further speculated that putrescine may promote EMT in GC cells by elevating *MAL2* via H3K27ac.

The effect of putrescine on GC cells via MAL2

To assess the influence of putrescine in *MAL2* expression, a western blot was employed to compare *MAL2* expression in GC cells with/without extracellular putrescine. We found that *MAL2* expression was significantly increased by extracellular putrescine in both AGS and MKN-28 cells (**Figure 6A**, **6B**). Subsequently, the roles of *MAL2* on EMT in GC cells were investigated. The Western blot analysis showed that introducing MAL2-specific shRNA into

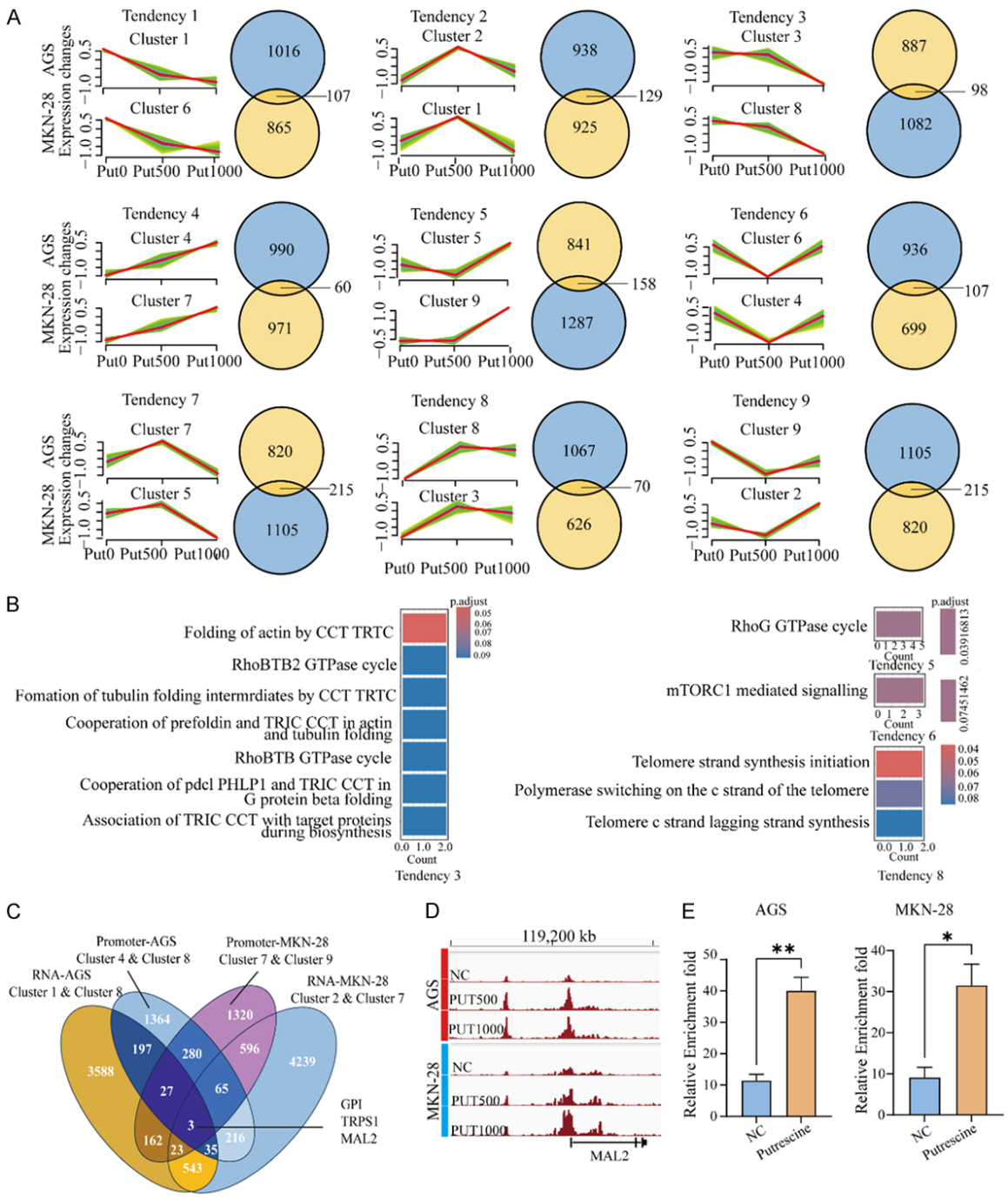

Figure 5. The combination analysis of transcriptome and CUT&Tag data. A. The diagrams illustrate the patterns of dynamic changes in promoter abundance along with the different concentrations of exogenous putrescine in AGS and MKN-28 cells, using Mfuzz. Venn diagram depicts the number of AGS and MKN-28 genes and the number of identical genes in the same trend; B. Pathway analysis showing the pathways enriched by shared genes within the same trend in Venn diagram; C. A Venn diagram illustrating the shared genes among the genes tending to increase in AGS and MKN-28 cells at RNA and promoter level; D. Normalized read densities for H3K27ac at the MAL2 on AGS and MKN-28 cells; E. The relative enrichment fold of H3K27ac level at the MAL2 promoter region in AGS and MKN-28 cells. Experiments were conducted in triplicate. Data are shown as mean ± SD. *P < 0.05, **P < 0.01, and ***P < 0.001.

AGS and MKN-28 cells, specifically MAL2-shRNAs-2# for AGS cells and MAL2-shRNAs-3# for MKN-28 cells, effectively reduced the expression of *MAL2* in both cell lines (**Figure**

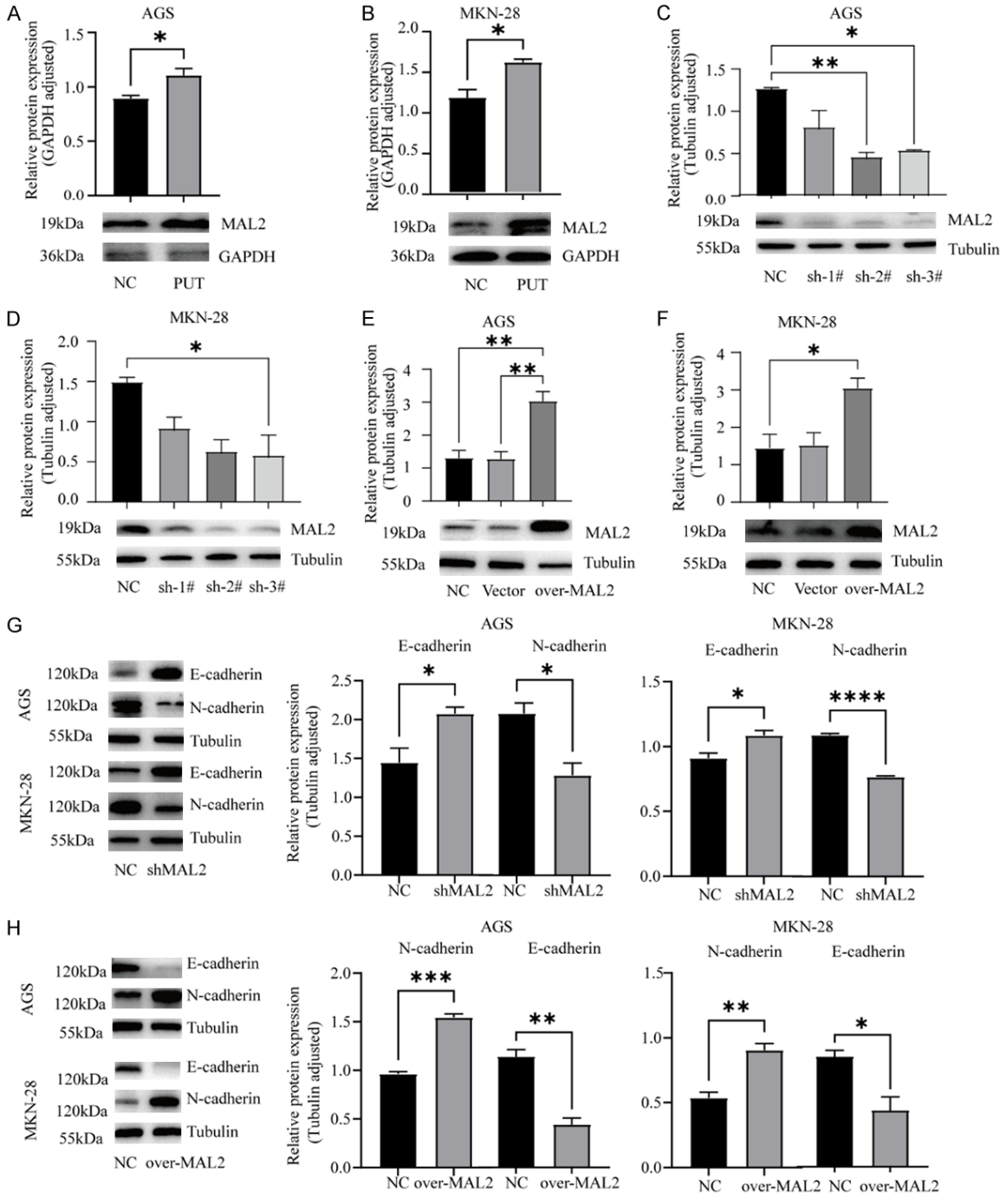

Figure 6. The roles of MAL2 in EMT of GC cells. A, B. MAL2 protein levels were compared between the Putrescine and Control groups through Western blot; C, D. AGS and MKN-28 cells were transfected with sh-MAL2-1#, sh-MAL2-2#, or sh-MAL2-3#, then the expression of MAL2 was assessed by western blot; E, F. AGS and MKN-28 cells were transfected with vector or flag-MAL2, and the expression of MAL2 was assessed by western blot; G. The protein expression levels of E-cadherin and N-cadherin were detected by western blot in AGS and MKN-28 cells after MAL2 knockdown; H. The protein expression levels of E-cadherin and N-cadherin were detected by western blot in AGS and MKN-28 cells after overexpression of MAL2. Experiments were conducted in triplicate. Data are shown as mean ± SD. **P* < 0.05, ***P* < 0.01, and ****P* < 0.001.

6C, **6D**). In addition, transfecting AGS and MKN-28 cells with *MAL2* Lentiviral Vector significantly overexpressed *MAL2* in both AGS and MKN-28 cells (**Figure 6E**, **6F**).

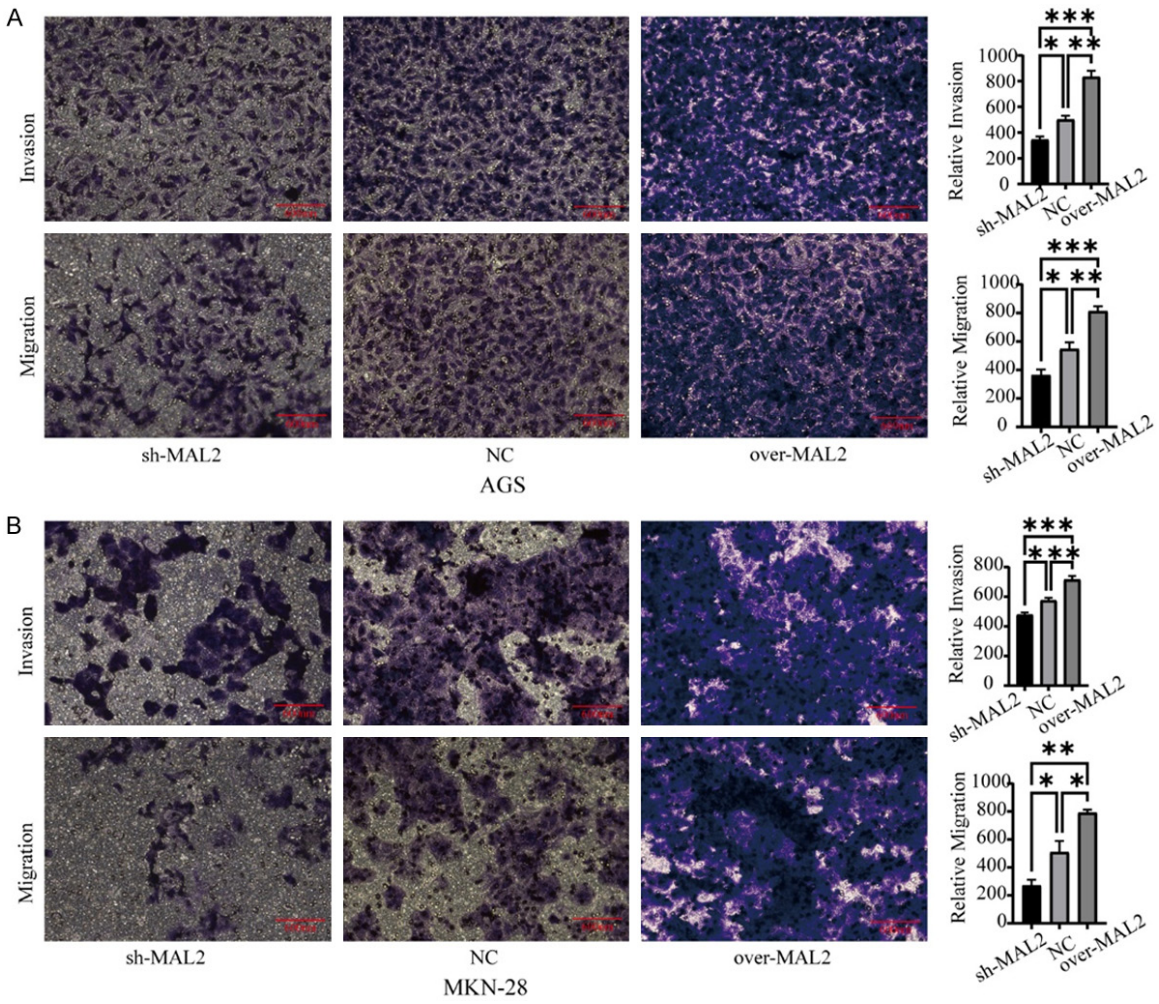

Figure 7. The roles of MAL2 in the migration and invasion of GC cells. A, B. The migration and invasion of AGS and MKN-28 cells were investigated by transwell assay under the effect of MAL2. Data are shown as mean ± SD. *P < 0.05, **P < 0.01, and ***P < 0.001.

The Western blot analysis demonstrated that *MAL2* knockdown significantly reduced N-cadherin expression (P < 0.05, AGS cells; P < 0.05, MKN-28 cell) and significantly increased the expression of E-cadherin (P < 0.05, AGS cells; P < 0.05, MKN-28 cells) compared to NC (**Figure 6G**). Moreover, overexpression of *MAL2* in AGS and MKN-28 cells led to a remarkable down-regulation of E-cadherin (P < 0.05, AGS cells; P < 0.05, MKN-28 cells) and upregulation of N-cadherin (P < 0.05, AGS cells; P < 0.05, MKN-28 cells) in MKN-28 and AGS cells lines (**Figure 6H**). The transwell assays also showed that sh-MAL2 remarkably weakened the invasion and migration of AGS and MKN-28 cells compared to NC, and overexpressing *MAL2* enhanced the invasion and migration of AGS and MKN-28 cells (**Figure 7A**, **7B**). Together, these results indicated that the expression of *MAL2* promotes EMT in GC cells.

Discussion

Studies have shown that polyamines play a complex role in tumor development [13]. The recent research on the regulatory effects of polyamines on gene expression in macrophages through histone modifications [40, 41] suggests that polyamines may also regulate gene expression in tumor cells by globally or selectively modifying histones. Previous research has extensively examined the connections between tumor growth and H3K27AC, as well as the metabolic processes involving polyamines in GC [22, 42]. However, no study has investigated whether putrescine can influence

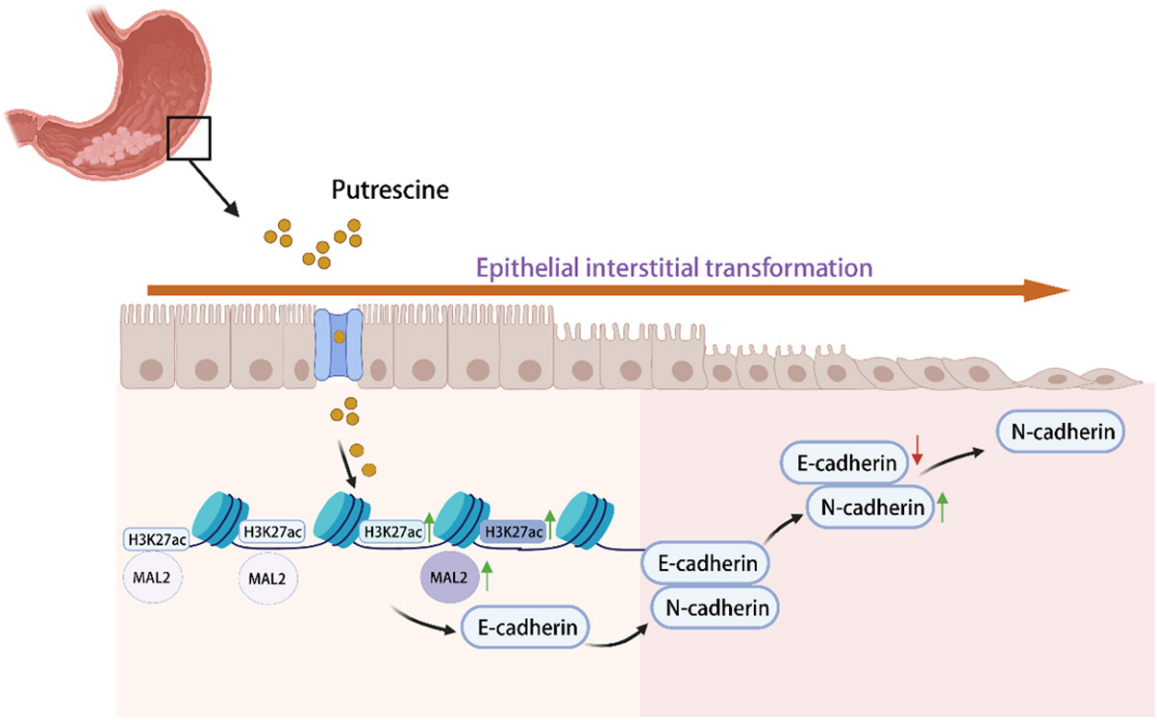

Figure 8. Diagram depicting the mechanism of extracellular putrescine on EMT in gastric cancer.

the malignant characteristics of GC by modifying H3K27ac on a global scale or in specific regions. In this study, our findings demonstrated that extracellular putrescine could promote malignant behavior of MKN-28 and AGS cells and elevate H3K27ac levels in the promoter region of *MAL2*, and upregulated *MAL2* could promote EMT in the two cell lines, validating that putrescine can upregulate *MAL2* expression by increasing H3K27ac level in its promoter region and subsequently promoting EMT in GC cells (**Figure 8**).

Previous studies have reported that colon cancer cells can uptake and release putrescine [43]. In this study, the decreased concentration of extracellular putrescine demonstrated its uptake by AGS and MKN-28 cells (**Figure 2C**), laying a foundation for further exploration. Previous studies have shown the necessary roles of polyamines in the proliferation of cancer cells, such as breast cancer and hepatoma cells [44-46]. In the colon, polyamines and their metabolizing enzymes could be reliable markers of neoplastic proliferation [47]. In this study, proliferation assays demonstrated the promotive effect of putrescine on GC cells (**Figure 2D**). ODC is a crucial enzyme in the polyamine biosynthetic pathway [48]. ODC promotes the invasiveness of colorectal cancer [48, 49], which is consistent with the finding in this study (**Figure 2E**, **2F**) that extracellular putrescine promoted invasion and migration of AGS. Furthermore, the results demonstrated that N1, N11-diethylnorspermine, an inducer of polyamine catabolism, could initiate EMT formation in hepaRG cells [50]. Moreover, the inhibition of AOC1, which catalyzes the deamination of polyamines, inhibited the EMT process [51]. These findings unveiled strong connections between EMT and polyamine metabolism. In this study, the MKN-28 representing the epithelial phenotype with high E-cadherin and low N-cadherin levels, and AGS representing the mesenchymal properties with low E-cadherin and high N-cadherin levels [23] were used to explore the influence of putrescine on the EMT of GC cells *in vitro*. The elevated N-cadherin and impaired E-cadherin levels in both cell lines strongly demonstrated the promotive roles of extracellular putrescine on the EMT of GC cells. Nevertheless, the oncogenic EMT and EMT-suppressive genes were present simultaneously in both the upregulated and downregulated genes in both cell lines, complicating further investigation into the underlying mechanisms.

In our initial hypothesis, putrescine could promote GC EMT by affecting H3K27ac. The experiments *in vivo* confirm that putrescine could promote EMT progression of GC by elevating H3K27ac (**Figure 4B**, **4C**). The elevated aerobic respiration relevant pathways (such as oxidative phosphorylation and ATP synthesis-coupled electron transport) might promote the protein acetylation [52], offering potential mechanisms on how extracellular putrescine upregulated H3K27ac expression in GC cells (**Figure 4A**). Extracellular putrescine has increased the expression of N-cadherin in both AGS and MKN-28 cells. However, it has only raised the expression of the global H3K27ac level in MKN-28 cells. This suggests that putrescine may influence the EMT of GC cells by affecting H3K27ac in specific regions. H3K27ac is correlated with the active enhancer modulatory elements to activate gene expression [4, 53], and the positive roles of H3K27ac in EMT have been widely recognized [11, 12]. Therefore, we investigated whether any shared downstream genes could be augmented by H3K27ac and promote EMT of GC cells. The CUT&Tag combined with RNA-seq can simultaneously profile histone post-translational modifications and gene expression in single cells [54, 55]. In this investigation, RNA-seq profiling of cellular transcriptomes was conducted on CUT&Tag capturing regions bound with H3K27ac to identify new putative EMT marker genes stimulated by extracellular putrescine and augmented by H3K27ac. Among all upregulated genes, there were three common genes - *GPI*, *TRPS1*, and *MAL2*. Glycosylphosphatidylinositol is a glycolipid anchor that can attach to the extracellular leaflet of the plasma membrane through a post-translational modification [36]. Previous studies have suggested that GPI-anchored proteins are involved in multiple cancers [37]. Trichorhinophalangeal syndrome type 1 is a marker for triple-negative breast cancer, which can suppress the EMT of breast cancer as a negative regulator [38, 39]. *MAL2* is a member of the MAL family of proteins with four transmembrane areas [56]. *MAL2* has been identified to be associated with the progression of multiple cancers. For example, high expression of *MAL2* promotes the proliferation of lung and ovarian cancer cells [57, 58] and encourages the development of pancreatic, colorectal, breast, and cervical cancers [57-60]. Furthermore, the overexpression of the MAL2 protein was anti-oncogenic and led to decreased cell migration, invasion, and viability in hepatic cells [61]. In addition, the predictive role of *MAL2* for distant metastasis in pancreatic cancer has been recognized [57]. However, little is known about the function of *MAL2* in GC. Our study found upregulation of E-cadherin and downregulation of N-cadherin after *MAL2* knockdown (**Figure 6G**). In contrast, the upregulation of N-cadherin and downregulation of E-cadherin were found after *MAL2* overexpression (**Figure 6H**), suggesting that *MAL2* could promote EMT in GC cells. Given that putrescine can enhance *MAL2* expression and increase H3K27ac levels in the promoter region of *MAL2* in GC cells, it is reasonable to conclude that putrescine can promote *MAL2* expression by elevating H3K27ac in its promoter region, leading to an increased occurrence of EMT in GC cells. However, our findings were observed mainly based on the cell lines and mice models, while the human relevance was unclear. In addition, more efforts should be made to extrapolate *in vitro* results to *in vivo* conditions and thoroughly investigate the molecular mechanisms and pathways.

Conclusions

We found that extracellular putrescine could promote malignant behavior and EMT of GC cells. The underlying mechanism was that extracellular putrescine could elevate H3K27ac in the promoter region of *MAL2*, which has been demonstrated to promote EMT of GC cells. Our study might provide new insights into the association between dietary polyamines and GC progression.

Acknowledgements

We want to thank Shaojie Shi and Xia Wei for their suggestions and help in the experiments. We also would like to thank FULI Instruments for its help and contribution to the experimental design of HPLC. This work was supported by the Shandong Provincial College Youth Innovation and Talent Cultivation Plan, the Natural Science Foundation of Shandong Province (ZR2023MC056), the Science and Technology project of Yantai (2023JCYJ070, 2023YD034), the Binzhou Medical University (50012304420), and the Natural Science

Foundation of Shandong Province (ZR2021-MH402).

Disclosure of conflict of interest

The authors declare that the research was performed without commercial or financial relationships that could be perceived as a potential conflict of interest.

Address correspondence to: Chengxia Liu, Department of Gastroenterology and Institute of Digestive Disease, Binzhou Medical University Hospital, Binzhou 256600, Shandong, China. E-mail: phdlcx@bzmc.edu.cn

References

[1] Sung H, Ferlay J, Siegel RL, Laversanne M, Soerjomataram I, Jemal A and Bray F. Global cancer statistics 2020: GLOBOCAN estimates of incidence and mortality worldwide for 36 cancers in 185 countries. CA Cancer J Clin 2021; 71: 209-249.

[2] Zhao X, Li K, Chen M and Liu L. Metabolic codependencies in the tumor microenvironment and gastric cancer: difficulties and opportunities. Biomed Pharmacother 2023; 162: 114601.

[3] Choi YJ, Kim N, Chang H, Lee HS, Park SM, Park JH, Shin CM, Kim JM, Kim JS, Lee DH and Jung HC. Helicobacter pylori-induced epithelial-mesenchymal transition, a potential role of gastric cancer initiation and an emergence of stem cells. Carcinogenesis 2015; 36: 553-63.

[4] Li J and Wang H. H3K27ac-activated EGFR-AS1 promotes cell growth in cervical cancer through ACTN4-mediated WNT pathway. Biol Direct 2022; 17: 3.

[5] Casero RA Jr, Murray Stewart T and Pegg AE. Polyamine metabolism and cancer: treatments, challenges and opportunities. Nat Rev Cancer 2018; 18: 681-695.

[6] Prunotto M, Compagnone A, Bruschi M, Candiano G, Colombatto S, Bandino A, Petretto A, Moll S, Bochaton-Piallat ML, Gabbiani G, Dimuccio V, Parola M, Citti L and Ghiggeri G. Endocellular polyamine availability modulates epithelial-to-mesenchymal transition and unfolded protein response in MDCK cells. Lab Invest 2010; 90: 929-39.

[7] Bello-Fernandez C, Packham G and Cleveland JL. The ornithine decarboxylase gene is a transcriptional target of c-Myc. Proc Natl Acad Sci U S A 1993; 90: 7804-8.

[8] Inamura N, Kimura T, Wang L, Yanagi H, Tsuda M, Tanino M, Nishihara H, Fukuda S and Tanaka S. Notch1 regulates invasion and metastasis of head and neck squamous cell carcinoma by inducing EMT through c-Myc. Auris Nasus Larynx 2017; 44: 447-457.

[9] Cipolla BG, Havouis R and Moulinoux JP. Polyamine reduced diet (PRD) nutrition therapy in hormone refractory prostate cancer patients. Biomed Pharmacother 2010; 64: 363-8.

[10] Bardócz S, Duguid TJ, Brown DS, Grant G, Pusztai A, White A and Ralph A. The importance of dietary polyamines in cell regeneration and growth. Br J Nutr 1995; 73: 819-28.

[11] Segelle A, Núñez-Álvarez Y, Oldfield AJ, Webb KM, Voigt P and Luco RF. Histone marks regulate the epithelial-to-mesenchymal transition via alternative splicing. Cell Rep 2022; 38: 110357.

[12] Song Y, Li ZX, Liu X, Wang R, Li LW and Zhang Q. The Wnt/beta-catenin and PI3K/Akt signaling pathways promote EMT in gastric cancer by epigenetic regulation via H3 lysine 27 acetylation. Tumour Biol 2017; 39: 1010428317712617.

[13] Wei G, Hobbs CA, Defeo K, Hayes CS and Gilmour SK. Polyamine-mediated regulation of protein acetylation in murine skin and tumors. Mol Carcinog 2007; 46: 611-7.

[14] Estepa I and Pestaña A. Activation by polyamines of the acetylation of endogenous histones in isolated chromatin and nuclei from Artemia. Eur J Biochem 1981; 119: 431-6.

[15] Dod B, Kervabon A and Parello J. Effect of cations on the acetylation of chromatin in vitro. Eur J Biochem 1982; 121: 401-5.

[16] Zanatta JM, Acuña SM, de Souza Angelo Y, de Almeida Bento C, Peron JPS, Stolf BS and Muxel SM. Putrescine supplementation shifts macrophage L-arginine metabolism related-genes reducing Leishmania amazonensis infection. PLoS One 2023; 18: e0283696.

[17] Goes EC, Cardoso Dal Pont G, Oliveira PR, da Rocha C and Maiorka A. Effects of putrescine injection in broiler breeder eggs. J Anim Physiol Anim Nutr (Berl) 2021; 105: 294-304.

[18] Newsome RC, Yang Y and Jobin C. The microbiome, gastrointestinal cancer, and immunotherapy. J Gastroenterol Hepatol 2022; 37: 263-272.

[19] Yang Y, Misra BB, Liang L, Bi D, Weng W, Wu W, Cai S, Qin H, Goel A, Li X and Ma Y. Integrated microbiome and metabolome analysis reveals a novel interplay between commensal bacteria and metabolites in colorectal cancer. Theranostics 2019; 9: 4101-4114.

[20] Farriol M, Segovia-Silvestre T, Castellanos JM, Venereo Y and Orta X. Role of putrescine in cell proliferation in a colon carcinoma cell line. Nutrition 2001; 17: 934-8.

[21] Linsalata M, Russo F, Notarnicola M, Berloco P and Di Leo A. Polyamine profile in human gas-

tric mucosa infected by Helicobacter pylori. Ital J Gastroenterol Hepatol 1998; 30: 484-9.
[22] McNamara KM, Gobert AP and Wilson KT. The role of polyamines in gastric cancer. Oncogene 2021; 40: 4399-4412.
[23] Yue B, Song C, Yang L, Cui R, Cheng X, Zhang Z and Zhao G. METTL3-mediated N6-methyladenosine modification is critical for epithelial-mesenchymal transition and metastasis of gastric cancer. Mol Cancer 2019; 18: 142.
[24] An L, Gong H, Yu X, Zhang W, Liu X, Yang X, Shu L, Liu J and Yang L. Downregulation of MAL2 inhibits breast cancer progression through regulating beta-catenin/c-Myc axis. Cancer Cell Int 2023; 23: 144.
[25] Huang P, Wang M, Lu Z, Shi S, Wei X, Bi C, Wang G, Liu H, Hu T and Wang B. Putrescine accelerates the differentiation of bone marrow derived dendritic cells via inhibiting phosphorylation of STAT3 at Tyr705. Int Immunopharmacol 2023; 116: 109739.
[26] Chen S, Zhou Y, Chen Y and Gu J. fastp: an ultra-fast all-in-one FASTQ preprocessor. Bioinformatics 2018; 34: i884-i890.
[27] Liao Y, Smyth GK and Shi W. featureCounts: an efficient general purpose program for assigning sequence reads to genomic features. Bioinformatics 2014; 30: 923-30.
[28] Love MI, Huber W and Anders S. Moderated estimation of fold change and dispersion for RNA-seq data with DESeq2. Genome Biol 2014; 15: 550.
[29] Subramanian A, Tamayo P, Mootha VK, Mukherjee S, Ebert BL, Gillette MA, Paulovich A, Pomeroy SL, Golub TR, Lander ES and Mesirov JP. Gene set enrichment analysis: a knowledge-based approach for interpreting genome-wide expression profiles. Proc Natl Acad Sci U S A 2005; 102: 15545-50.
[30] Wu T, Hu E, Xu S, Chen M, Guo P, Dai Z, Feng T, Zhou L, Tang W, Zhan L, Fu X, Liu S, Bo X and Yu G. clusterProfiler 4.0: a universal enrichment tool for interpreting omics data. Innovation (Camb) 2021; 2: 100141.
[31] Kumar L and E Futschik M. Mfuzz: a software package for soft clustering of microarray data. Bioinformation 2007; 2: 5-7.
[32] Langmead B, Wilks C, Antonescu V and Charles R. Scaling read aligners to hundreds of threads on general-purpose processors. Bioinformatics 2019; 35: 421-432.
[33] Yu G, Wang LG and He QY. ChIPseeker: an R/Bioconductor package for ChIP peak annotation, comparison and visualization. Bioinformatics 2015; 31: 2382-3.
[34] Zhao M, Liu Y, Zheng C and Qu H. dbEMT 2.0: an updated database for epithelial-mesenchymal transition genes with experimentally verified information and precalculated regulation information for cancer metastasis. J Genet Genomics 2019; 46: 595-597.
[35] Hu G, Ma J, Zhang J, Chen Y, Liu H, Huang Y, Zheng J, Xu Y, Xue W and Zhai W. Hypoxia-induced lncHILAR promotes renal cancer metastasis via ceRNA for the miR-613/206/1-1-3p/Jagged-1/Notch/CXCR4 signaling pathway. Mol Ther 2021; 29: 2979-2994.
[36] Lebreton S, Zurzolo C and Paladino S. Organization of GPI-anchored proteins at the cell surface and its physiopathological relevance. Crit Rev Biochem Mol Biol 2018; 53: 403-419.
[37] Gamage DG and Hendrickson TL. GPI transamidase and GPI anchored proteins: oncogenes and biomarkers for cancer. Crit Rev Biochem Mol Biol 2013; 48: 446-64.
[38] Ai D, Yao J, Yang F, Huo L, Chen H, Lu W, Soto LMS, Jiang M, Raso MG, Wang S, Bell D, Liu J, Wang H, Tan D, Torres-Cabala C, Gan Q, Wu Y, Albarracin C, Hung MC, Meric-Bernstam F, Wistuba II, Prieto VG, Sahin AA and Ding Q. TRPS1: a highly sensitive and specific marker for breast carcinoma, especially for triple-negative breast cancer. Mod Pathol 2021; 34: 710-719.
[39] Hu J, Su P, Jiao M, Bai X, Qi M, Liu H, Wu Z, Sun J, Zhou G and Han B. TRPS1 suppresses breast cancer epithelial-mesenchymal transition program as a negative regulator of SUZ12. Transl Oncol 2018; 11: 416-425.
[40] Sakamoto A, Terui Y, Uemura T, Igarashi K and Kashiwagi K. Polyamines regulate gene expression by stimulating translation of histone acetyltransferase mRNAs. J Biol Chem 2020; 295: 8736-8745.
[41] Latour YL, Gobert AP and Wilson KT. The role of polyamines in the regulation of macrophage polarization and function. Amino Acids 2020; 52: 151-160.
[42] Zhang Y, Liu Z, Yang X, Lu W, Chen Y, Lin Y, Wang J, Lin S and Yun JP. H3K27 acetylation activated-COL6A1 promotes osteosarcoma lung metastasis by repressing STAT1 and activating pulmonary cancer-associated fibroblasts. Theranostics 2021; 11: 1473-1492.
[43] McCormack SA and Johnson LR. Putrescine uptake and release by colon cancer cells. Am J Physiol 1989; 256: G868-77.
[44] Akinyele O and Wallace HM. Understanding the polyamine and mTOR pathway interaction in breast cancer cell growth. Med Sci (Basel) 2022; 10: 51.
[45] Gerner EW and Mamont PS. Restoration of the polyamine contents in rat hepatoma tissue-culture cells after inhibition of polyamine biosynthesis. Relationship with cell proliferation. Eur J Biochem 1986; 156: 31-5.
[46] Akinyele O and Wallace HM. Characterising the response of human breast cancer cells to poly-

amine modulation. Biomolecules 2021; 11: 743.
[47] Milovic V and Turchanowa L. Polyamines and colon cancer. Biochem Soc Trans 2003; 31: 381-3.
[48] Zhang B, Liu XX, Zhang Y, Jiang CY, Hu HY, Gong L, Liu M and Teng QS. Polyamine depletion by ODC-AdoMetDC antisense adenovirus impairs human colorectal cancer growth and invasion in vitro and in vivo. J Gene Med 2006; 8: 980-9.
[49] Auvinen M. Cell transformation, invasion, and angiogenesis: a regulatory role for ornithine decarboxylase and polyamines? J Natl Cancer Inst 1997; 89: 533-7.
[50] Ivanova ON, Snezhkina AV, Krasnov GS, Valuev-Elliston VT, Khomich OA, Khomutov AR, Keinanen TA, Alhonen L, Bartosch B, Kudryavtseva AV, Kochetkov SN and Ivanov AV. Activation of polyamine catabolism by N(1),N(11)-diethylnorspermine in hepatic HepaRG cells induces dedifferentiation and mesenchymal-like phenotype. Cells 2018; 7: 275.
[51] Xu F, Xu Y, Xiong JH, Zhang JH, Wu J, Luo J and Xiong JP. AOC1 contributes to tumor progression by promoting the AKT and EMT pathways in gastric cancer. Cancer Manag Res 2020; 12: 1789-1798.
[52] Jin J, Zhang L, Li X, Xu W, Yang S, Song J, Zhang W, Zhan J, Luo J and Zhang H. Oxidative stress-CBP axis modulates MOB1 acetylation and activates the Hippo signaling pathway. Nucleic Acids Res 2022; 50: 3817-3834.
[53] Creyghton MP, Cheng AW, Welstead GG, Kooistra T, Carey BW, Steine EJ, Hanna J, Lodato MA, Frampton GM, Sharp PA, Boyer LA, Young RA and Jaenisch R. Histone H3K27ac separates active from poised enhancers and predicts developmental state. Proc Natl Acad Sci U S A 2010; 107: 21931-6.
[54] Zhu C, Zhang Y, Li YE, Lucero J, Behrens MM and Ren B. Joint profiling of histone modifications and transcriptome in single cells from mouse brain. Nat Methods 2021; 18: 283-292.
[55] Liorni N, Napoli A, Castellana S, Giallongo S, Řeháková D, Re OL, Koutná I, Mazza T and Vinciguerra M. Integrative CUT&Tag-RNA-Seq analysis of histone variant macroH2A1-dependent orchestration of human induced pluripotent stem cell reprogramming. Epigenomics 2023; 15: 863-877.
[56] Frank M. MAL, a proteolipid in glycosphingolipid enriched domains: functional implications in myelin and beyond. Prog Neurobiol 2000; 60: 531-44.
[57] Zhang B, Xiao J, Cheng X and Liu T. MAL2 interacts with IQGAP1 to promote pancreatic cancer progression by increasing ERK1/2 phosphorylation. Biochem Biophys Res Commun 2021; 554: 63-70.
[58] Li J, Li Y, Liu H, Liu Y and Cui B. The four-transmembrane protein MAL2 and tumor protein D52 (TPD52) are highly expressed in colorectal cancer and correlated with poor prognosis. PLoS One 2017; 12: e0178515.
[59] Chen L, Li H, Yao D, Zou Q, Yu W and Zhou L. The novel circ_0084904/miR-802/MAL2 axis promotes the development of cervical cancer. Reprod Biol 2022; 22: 100600.
[60] Bhandari A, Shen Y, Sindan N, Xia E, Gautam B, Lv S and Zhang X. MAL2 promotes proliferation, migration, and invasion through regulating epithelial-mesenchymal transition in breast cancer cell lines. Biochem Biophys Res Commun 2018; 504: 434-439.
[61] López-Coral A, Del Vecchio GJ, Chahine JJ, Kallakury BV and Tuma PL. MAL2-induced actin-based protrusion formation is anti-oncogenic in hepatocellular carcinoma. Cancers (Basel) 2020; 12: 422.